nature physics

SUPPLEMENTARY INFORMATION

DOI: 10.1038/NPHYS3244

Quantum distillation and confinement of vacancies in a doublon sea

Lin Xia[1], Laura A. Zundel[1], Juan Carrasquilla[1,2], Aaron Reinhard[1], Joshua M. Wilson[1], Marcos Rigol[1], and David S. Weiss[1]

[1]*Department of Physics, The Pennsylvania State University, University Park, PA 16802, USA*
[2]*Perimeter Institute for Theoretical Physics, Waterloo, Ontario, Canada N2L 2Y5*

Experiments

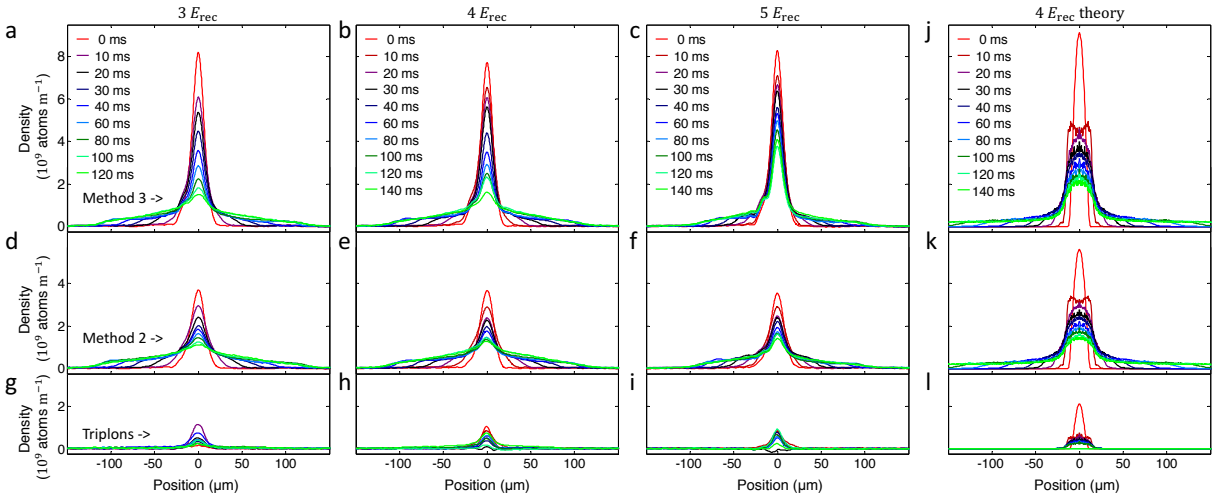

Figure S1 Spatial dynamics in the flat lattice. a-c. M3 measurements of atom distributions after three-body inelastic collisions have emptied triplon sites and most atoms from more highly occupied sites. **d-f**. M2 measurements of atom distributions after photoassociation. These distributions are approximately the same as the distributions of singlons. **g-i**. The distributions of triplons. These are derived from combining the raw measurements according to the formula M1-M3. Note that all the experimental plots (**a-i**) have the same vertical scale, and results are reported at successive t_{ev} at V_0=3E_{rec} (panels in the first column), 4E_{rec} (panels in the second column), and 5E_{rec} (panels in the third column). For a discussion of the small asymmetry in these figures, see Methods. **j-l.** Gutzwiller mean-field theory results for $V_0 = 4E_{rec}$ for M3, M1, and triplons, respectively.

DOI: 10.1038/NPHYS3244

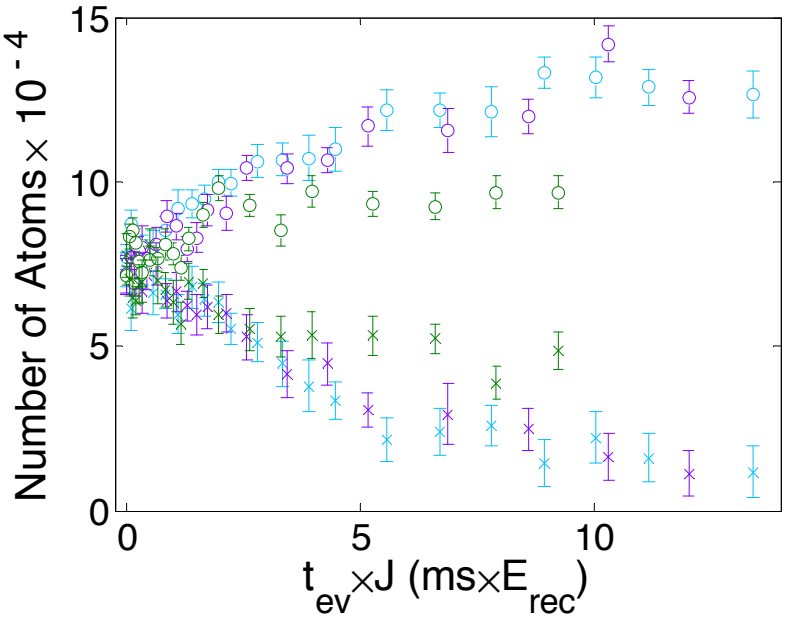

Figure S2 The time-rescaled loss of doublons. The experimental data from Fig. 3a-3b is replotted with the time axis scaled by J. The doublon populations are denoted by $\times$'s, and the singlon populations by open circles. The blue, purple and green symbols are from $V_0 = 3E_{\text{rec}}$, $4E_{\text{rec}}$, and $5E_{\text{rec}}$ respectively. The curves are approximately self-similar up until $\sim$3ms-E_{rec}, which suggests that doublon decay is predominantly a first-order process. The largest difference in the curves is that when the lattice is deeper, the doublons stop decaying at an earlier time, leaving a larger asymptotic doublon population.

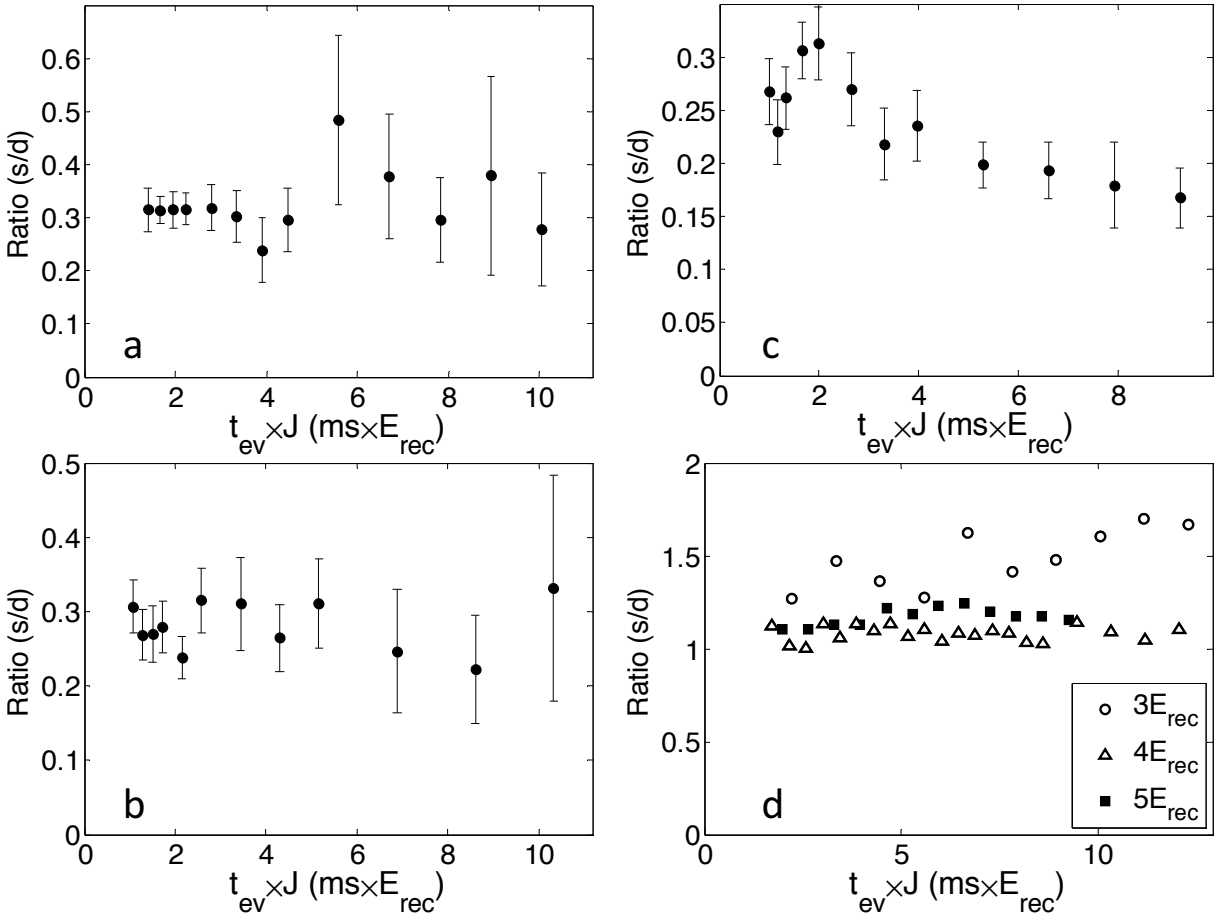

Figure S3 The ratio of trapped singlons to doublons. **a.** $3E_{\mathrm{rec}}$ experimental data, derived from data in Figs. 3a and 4a. **b.** $4E_{\mathrm{rec}}$ experimental data, derived from data in Figs. 3b and 4a. **c.** $5E_{\mathrm{rec}}$ experimental data, derived from data in Figs. 3c and 4a. **d.** Theoretical results for the ratio of trapped singlons to doublons at the three lattice depths, derived from Gutzwiller mean field calculations in the same way as the corresponding results are derived from the experimental data. The downward trend in **c** is the most direct signature of quantum distillation, since the number of trapped singlons decreases more quickly than the number of doublon atoms. Because at the lower lattice depths the number of doublons continues to decrease by dissolution into singlons, the fact that the ratios in **a** and **b** are approximately constant also implies that quantum distillation is occurring there. Most of the new singlons from doublon dissolution quantum distill out, along with enough of the old singlon to keep pace with the decreasing number of doublon atoms. The theory results here can be understood in a similar way, noting that at the higher two depths, there is both less doublon dissolution and less quantum distillation than in the experiment. We suspect that the dominant reason for quantitative disagreements between the experiment and the theory is the initial condition. The theory distributions are initially colder, which leads to an initial density-dropping expansion of all the atoms, and thus a lower central density (with more singlons and empty sites) throughout the rest of the evolution.

DOI: 10.1038/NPHYS3244

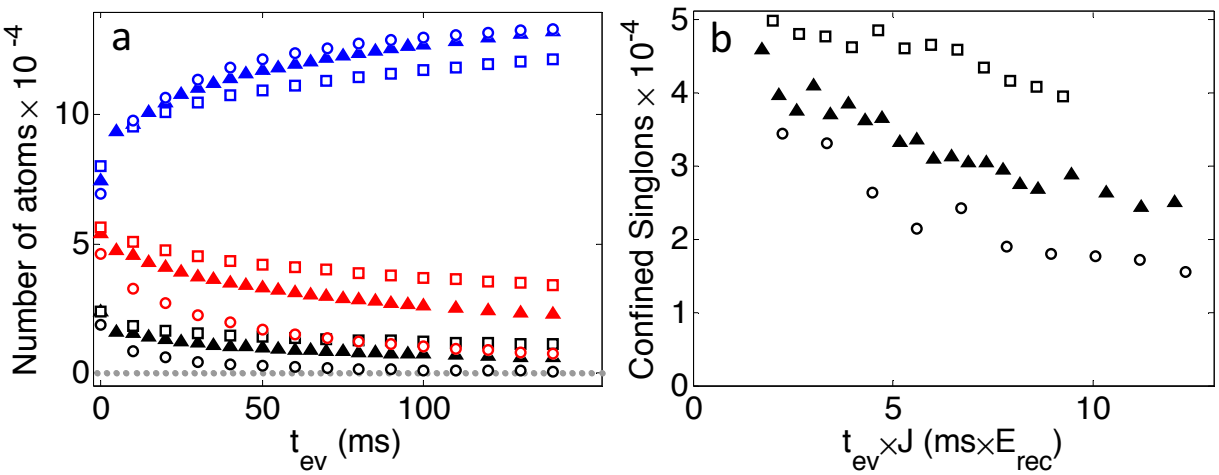

Figure S4 Theoretical evolution curves. a. The numbers of doublons (red), singlons (blue), and triplons (black) vs. evolution time. The circles are for $V = 3E_{\text{rec}}$, the triangles are for $V = 4E_{\text{rec}}$, and the squares are for $V = 5E_{\text{rec}}$. **b.** The number of confined singlons vs. time, with data labels as in **a**. As with the theory shown in the body of the paper, there are strong qualitative similarities with the experimental data. Comparison of **a** to Fig. 3 suggests that the strong difference in the extent of doublon dissolution between $4E_{\text{rec}}$ and $5E_{\text{rec}}$ in the experiment is shifted to between $3E_{\text{rec}}$ and $4E_{\text{rec}}$ in the theory. As with the other quantitative disagreements we see, we suspect the initial conditions, which give rise to more initial expansion at the deeper lattice depths. The curves in **b** do not overlap each other like those in Fig. 4b. Unlike in the experiment, where the initial spatial distributions do not significantly vary with lattice depth, they do in the theory calculations.

Theory

We assume that the system under consideration can be described in terms of particles moving in an array of independent 1D tubes. This is justified because the tunneling amplitude between adjacent tubes is exponentially small in the strength of the optical lattice defining the array, which in the experiment is $V_{\text{transverse}}/E_{\text{rec}} = 40$. The Hamiltonian in each 1D tube is

$$\begin{aligned}\mathcal{H} &= \int dz\psi^{\dagger}(z)\left[-\frac{\hbar^2}{2m}\frac{d^2}{dz^2}+V(z)\right]\psi(z)+\frac{1}{2}\int dz\psi^{\dagger}(z)\psi^{\dagger}(z')U(z-z')\psi(z')\psi(z)\\ &- \mu\int dz\psi^{\dagger}(z)\psi(z), \end{aligned} \tag{1}$$

where the field operators satisfy $[\psi(z),\psi^{\dagger}(z')] = \delta(z-z')$. The particles in each tube are subjected to a local potential due to the optical lattice and to an axial confinement potential, i.e., $V(z) = V_0\sin^2\left(\frac{2\pi}{\lambda}z\right)+\frac{1}{2}m\omega_z^2z^2$. The optical lattice is characterized by its depth V_0 and wavelength λ. The axial confinement is characterized by the frequency ω_z and the mass m of the Rb^{87} atoms. It is further assumed that the particles interact via a short-range potential $U(z-z') = g_{1D}\delta(z-z')$.[1] The chemical potential μ controls the total number of particles in the tube. In order to study the Hamiltonian in Eq. (1), one can then map the problem onto a simplified one-band Bose-Hubbard model,[2] which is a good approximation when the lattice is deep enough so that multiband effects can be neglected. Alternatively, it is possible to account for such effects, that are potentially relevant for the lowest lattice depths considered in the experiments, by introducing a grid spacing $\ell = \lambda/T$ to obtain the following "artificial" lattice Hamiltonian[3]

$$\begin{aligned}\mathcal{H}_{\text{BH}} &= -t_h\sum_i\left(b_i^{\dagger}b_{i+1}+h.c\right)+\frac{U_b}{2}\sum_i n_i(n_i-1)+V_0\sum_i\sin^2\left(\frac{2\pi}{T}i\right)n_i+\Omega_z\sum_i i^2n_i\\ &- \tilde{\mu}\sum_i n_i, \end{aligned} \tag{2}$$

where we have identified $b_i^{\dagger} = \psi^{\dagger}(i\ell)/\sqrt{\ell}$. Here, the hopping matrix element $t_h = E_{\text{rec}}\left(\frac{T}{2\pi}\right)^2$, the interaction $U_b = g_{1D}\frac{T}{\lambda}$, and the amplitude of the axial trapping potential is given by $\Omega_z = \frac{1}{2}m\omega_z^2\left(\frac{\lambda}{T}\right)^2$. Notice that the original Hamiltonian Eq. (1) is recovered in the limit $\mathcal{H} = \lim_{\ell\to 0}\mathcal{H}_{\text{BH}}$. In our simulations, however, we consider a finite $\ell = 0.05\lambda$ and ensure that the results are robust upon further increase of T. The coupling strength g_{1D} is estimated following Ref. 1 based on the parameters of the experimental setup. The effective chemical potential of each independent tube $\tilde{\mu} = \mu - \left(\frac{T}{\lambda}\right)^2$ is obtained by adding an energy offset due to the transverse parabolic trapping potential (which is characterized by its frequency ω_{xy}) to the overall chemical potential of the system. The latter is, in turn, fixed by total number of particles in the experiments. We simulate arrays of up to 110×110 tubes, each tube being 1000ℓ long. The axial size of the system is chosen so that the expanding particles never reach the edges of the tubes in the time scales of the simulation. The initial state ($t_{\text{ev}} = 0$) is assumed to be the ground state in the absence of tunneling between the 1D tubes. We tune the $t_{\text{ev}} = 0$ axial and transverse trapping potentials

DOI: 10.1038/NPHYS3244

(using the experimental value for their ratio) so that the initial fraction of singlons in the simulation matches the experiment. The lattice parameters are those of the experiment. For $t_{\mathrm{ev}} \geq 0$ the overall confining potential is set to zero exactly. All calculations are carried out using a Gutzwiller mean-field approach detailed in Refs. 4, 5.

The parameters U/J that correspond to the one-band Bose-Hubbard model discussed in the main text were obtained using maximally-localized generalized Wannier states[6] through the software available in Ref. 7.

1. Olshanii, M. Atomic scattering in the presence of an external confinement and a gas of impenetrable bosons. *Phys. Rev. Lett.* **81**, 938–941 (1998).

2. Fisher, M. P. A., Weichman, P. B., Grinstein, G. & Fisher, D. S. Boson localization and the superfluid-insulator transition. *Phys. Rev. B* **40**, 546–570 (1989).

3. Stoudenmire, E. M., Wagner, L. O., White, S. R. & Burke, K. One-dimensional continuum electronic structure with the density-matrix renormalization group and its implications for density-functional theory. *Phys. Rev. Lett.* **109**, 056402 (2012).

4. Jaksch, D., Venturi, V., Cirac, J. I., Williams, C. J. & Zoller, P. Creation of a molecular condensate by dynamically melting a Mott insulator. *Phys. Rev. Lett.* **89**, 040402 (2002).

5. Jreissaty, A., Carrasquilla, J. & Rigol, M. Self-trapping in the two-dimensional Bose-Hubbard model. *Phys. Rev. A* **88**, 031606 (2013).

6. Walters, R., Cotugno, G., Johnson, T. H., Clark, S. R. & Jaksch, D. *Ab initio* derivation of Hubbard models for cold atoms in optical lattices. *Phys. Rev. A* **87**, 043613 (2013).

7. Johnson, T., Clark, S., & Cotugno, G. Wannier states for optical lattices (2013). URL `http://ccpforge.cse.rl.ac.uk/gf/project/mlgws/`.